INTERNATIONAL JOURNAL FOR NUMERICAL METHODS IN ENGINEERING
Int. J. Numer. Meth. Engng 2004; **59**:1119–1136 (DOI: 10.1002/nme.908)

Combined extended and superimposed finite element method for cracks

Sang-Ho Lee[1,*,†], Jeong-Hoon Song[1], Young-Cheol Yoon[2], Goangseup Zi[2] and Ted Belytschko[2]

[1]*School of Civil and Environmental Engineering, Yonsei University, 134 Shinchon-Dong, Seodaemoon-Ku, Seoul 120-749, Korea*
[2]*Department of Mechanical Engineering, Northwestern University, 2145 Sheridan Road, Evanston, IL 60208-3111, U.S.A.*

SUMMARY

A combination of the extended finite element method (XFEM) and the mesh superposition method (s-version FEM) for modelling of stationary and growing cracks is presented. The near-tip field is modelled by superimposed quarter point elements on an overlaid mesh and the rest of the discontinuity is implicitly described by a step function on partition of unity. The two displacement fields are matched through a transition region. The method can robustly deal with stationary crack and crack growth. It simplifies the numerical integration of the weak form in the Galerkin method as compared to the s-version FEM. Numerical experiments are provided to demonstrate the effectiveness and robustness of the proposed method. Copyright © 2004 John Wiley & Sons, Ltd.

KEY WORDS: extended finite element; mesh superposition; crack

1. INTRODUCTION

Recently, a variation of the finite element method, the extended finite element method (XFEM), was developed to implicitly model internal discontinuities, such as cracks on the basis of the partition of unity [1–5]. The XFEM has proven quite successful in elastic fracture mechanics and in the treatment of cohesive crack models [6, 7]. This method can treat a crack that is arbitrary aligned with the mesh, so no remeshing is needed to model crack growth. As a result, the method can avoid difficulties that might ensue in remeshing when tracking crack growth. However, the treatment of the crack tip entails the use of asymptotic near-tip fields. These

*Correspondence to: Sang-Ho. Lee, School of Civil and Environmental Engineering, Yonsei University, 134 Shinchon-Dong, Seodaemoon-Ku, Seoul 120-749, Korea.
†E-mail: lee@yonsei.ac.kr

Contract/grant sponsor: Korea Research Foundation; contract/grant number: KRF-2002-042-D00115
Contract/grant sponsor: U.S. Office of Naval Research

Received 11 March 2003
Revised 1 May 2003
Accepted 20 June 2003

fields are sometimes difficult to integrate; their matching with the step function that models the remainder of the discontinuity is also at times problematic [8]. In this paper, we explore a method where the crack tip is treated by superimposed quarter point elements, whereas the rest of the crack is treated by the XFEM.

The concept of superposing a cracked mesh on a continuous mesh has been proposed by Fish in the s-method [9–11], an extension of the spectral overlay technique by Belytschko *et al.* [12]. A difficulty with the s-method is that quadrature of the Galerkin weak form becomes awkward because of the many discontinuities. Furthermore, intermediate elements need to be inserted when crack growth is modelled. The attractive feature of the proposed method is that the XFEM is used for the crack away from the tip. Therefore, no elements need to be inserted for crack growth. Furthermore, the quadrature tends to be simpler. Thus the proposed method can be viewed as a combination, or hybrid, or the s-method and XFEM. Therefore, we will call this XS-FEM in this paper.

2. SUPERIMPOSED DISPLACEMENT FIELDS FOR CRACK MODELLING

Consider a domain Ω with boundary $\partial\Omega$ and a crack Γ_C. The boundary consists of the prescribed traction boundary $\partial\Omega_t$ and the prescribed displacement boundary $\partial\Omega_u$; $\partial\Omega_u \cup \partial\Omega_t = \partial\Omega$ and $\partial\Omega_u \cap \partial\Omega_t = 0$ as shown in Figure 1. We allow this domain to contain discontinuities. Consider arbitrary regions completely enclosing the crack tips, we call these overlaid domains Ω_i^{ov} where i identifies the crack tip and $\Omega^{ov} = \bigcup_{i=1}^{N_c} \Omega_i^{ov}$. Each overlaid domain Ω_i^{ov} covers the region where the near-tip field of crack i is dominant and N_c indicates the number of crack tips. We assume that near-tip field is dominant only in this domain. Those domains are discretized independently with separate mesh structures.

On the basic mesh, the displacement field takes the form

$$\mathbf{u}^{ba}(\mathbf{x}) = \mathbf{u}^{cont}(\mathbf{x}) + \mathbf{u}^{disc}(\mathbf{x}), \quad \mathbf{x} \in \Omega \tag{1}$$

in which $\mathbf{u}^{cont}(\mathbf{x})$ represents the continuous displacement field and $\mathbf{u}^{disc}(\mathbf{x})$ denotes the discontinuous displacement field that is discontinuous across the crack. On the other hand, the displacement field on the overlaid mesh is defined by $\mathbf{u}^{ov}(\mathbf{x})$. The total displacement field is obtained by a superposition of two displacement fields of the separate meshes and it takes the form

$$\mathbf{u}(\mathbf{x}) = \mathbf{u}^{cont}(\mathbf{x}) + \mathbf{u}^{disc}(\mathbf{x}) + \mathbf{u}^{ov}(\mathbf{x}) \tag{2}$$

Let the boundary of each overlaid domain be Γ_i^{int}. We require that

$$\mathbf{u}^{ov}(\mathbf{x}) = 0, \quad \mathbf{x} \in \Gamma^{int} \tag{3}$$

In other words, $\mathbf{u}^{ov}(\mathbf{x})$ should vanish on $\Gamma^{int} (= \bigcup_{i=1}^{N_c} \Gamma_i^{int})$ to guarantee C^0 continuity of the total displacement field.

When the overlaid mesh completely falls within the domain i.e. $\partial\Omega_u \cap \Gamma_i^{int} = 0$, the essential boundary condition can be satisfied by the usual finite element method procedure. The prescribed displacement $\bar{\mathbf{u}}(\mathbf{x})$ can be approximated with

$$\mathbf{u}^{cont}(\mathbf{x}) = \bar{\mathbf{u}}(\mathbf{x}), \quad \mathbf{x} \in \partial\Omega_u \tag{4}$$

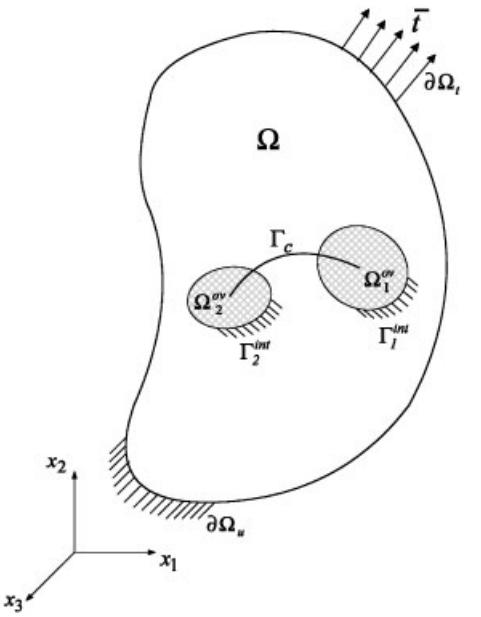

Figure 1. Basic domain (Ω) and overlaid domains ($\Omega_i^{\text{ov}},\ i=1,2$) in the XS-FEM.

However, if $\partial\Omega_u \cap \Gamma^{\text{int}} \neq 0$ then the prescribed displacement boundary condition is

$$\mathbf{u}^{\text{cont}}(\mathbf{x}) + \mathbf{u}^{\text{ov}}(\mathbf{x}) = \bar{\mathbf{u}}(\mathbf{x}) \quad \mathbf{x} \in \partial\Omega_u \cap \Gamma^{\text{int}} \tag{5}$$

The finite element approximation is constructed by meshing Ω and Ω^{ov} independently and superimposing the meshes. The domains Ω and Ω^{ov} are discretized by separate sets of elements Ω_e and Ω^{ov} such that

$$\bigcup_{e\in E} \Omega_e = \Omega \tag{6}$$

$$\bigcup_{e\in E^{\text{ov}}} \Omega_e^{\text{ov}} = \Omega^{\text{ov}} \tag{7}$$

where E and E^{ov} are the total ordering of the elements corresponding to basic and overlaid domains.

Figure 2 shows a mesh for the basic and overlaid meshes in XS-FEM. As can be seen, the near-tip field is modelled by a set of special elements for the crack on the overlaid mesh whereas the rest of the crack discontinuity is treated by the XFEM. Let the set of nodes of the basic mesh be Λ and the set of nodes of the overlaid mesh be $\Lambda^{\text{ov}} = \bigcup_{i=1}^{N_C} \Lambda_i^{\text{ov}}$. On the basic mesh, the XS-FEM approximation, which has only step function enrichment, can be written as

$$\begin{aligned}\hat{\mathbf{u}}^{\text{ba}}(\mathbf{x}) &= \hat{\mathbf{u}}^{\text{cont}}(\mathbf{x}) + \hat{\mathbf{u}}^{\text{disc}}(\mathbf{x}) \\ &= \sum_{I\in\Lambda} N_I(\mathbf{x})\mathbf{u}_I + \sum_{J\in\Lambda_{\text{disc}}} N_J(\mathbf{x})\Psi(\mathbf{x})\mathbf{a}_J, \quad \mathbf{x}\in\Omega\end{aligned} \tag{8}$$

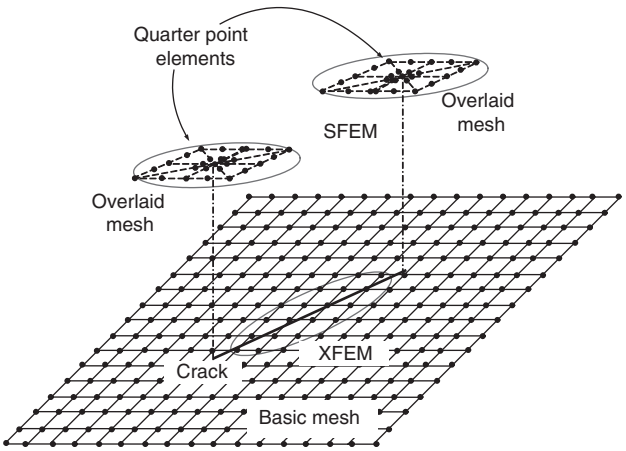

Figure 2. Mesh discretization of the basic and overlaid domains in the XS-FEM; the near-tip field of the overlaid domain is modelled by quarter point elements and the rest of the crack is treated by the XFEM on the basic mesh.

where $\mathbf{u}_I$ are displacement vector at the basic mesh nodes, $\mathbf{a}_J$ are enrichment parameters that give the strength of discontinuity, and Λ_{disc} is the set of nodes that are to be enriched with step functions. $\Psi(\mathbf{x})$ are discontinuous enrichment functions for the elements completely cut by a crack. To form a local partition of unity the enriched displacement field should vanish outside the enriched element [13]. Thus, a shifted sign function [7] is used

$$\Psi(\mathbf{x}) = \text{sign}(\phi(\mathbf{x})) - \text{sign}(\phi(\mathbf{x}_J)), \quad J \in \Lambda_{\text{disc}} \tag{9}$$

where $\phi(\mathbf{x})$ is a level set function constructed from the signed distance function; it is defined by

$$\phi(\mathbf{x}) = \min_{\mathbf{y}\in\Gamma_C} (\mathbf{x} - \mathbf{y}) \, \text{sign}(\mathbf{n} \bullet (\mathbf{x} - \mathbf{y})) \tag{10}$$

The sign function is defined by

$$\text{sign}(x) = \begin{cases} -1 & \text{for } x < 0 \\ +1 & \text{for } x > 0 \end{cases} \tag{11}$$

Thus, the crack is implicitly defined by the level set function and the end points of the crack. Other applications of step function for elements completely cut by a crack can be found in References [2–5].

The finite element approximation on the overlaid mesh takes the form

$$\hat{\mathbf{u}}^{\text{ov}}(\mathbf{x}) = \sum_{K\in\Lambda^{\text{ov}}} N_K^{\text{ov}}(\mathbf{x})\mathbf{c}_K, \quad \mathbf{x} \in \Omega^{\text{ov}} \tag{12}$$

where $\mathbf{c}_K$ represents near-tip field displacement on the overlaid mesh and $N_K^{\text{ov}}(\mathbf{x})$ denotes the shape function of the element chosen to model the crack tip. Here we have used the triangular quarter point element that is constructed by coalescing eight-node quarter point element [14].

It is well known that the derivative of $N_K^{\mathrm{ov}}(\mathbf{x})$ has an $r^{-1/2}$ singularity at the crack tip. From (8) and (12), the complete approximation reads

$$\hat{\mathbf{u}}(\mathbf{x}) = \sum_{I\in\Lambda} N_I(\mathbf{x})\mathbf{u}_I + \sum_{J\in\Lambda_{\mathrm{disc}}} N_J(\mathbf{x})\Psi(\mathbf{x})\mathbf{a}_J + \sum_{K\in\Lambda^{\mathrm{ov}}} N_K^{\mathrm{ov}}(\mathbf{x})\mathbf{c}_K, \quad \mathbf{x}\in\Omega \tag{13}$$

Chessa *et al.* [13] pointed out that a local partition of unity loses the reproducing property in the region where the enriched elements are blended with standard finite elements. In this work, this difficulty does not arise because only the step function is used to enrich the approximation by the local partition of unity. The near-tip field in (12) totally participates in approximation (13) when it matches with (8) over $\Omega\cap\Omega^{\mathrm{ov}}$, i.e. it is simply added to the approximation directly rather than through a partition of unity. Therefore, higher-order approximations do not cause a difficulty as in Stazi *et al.* [8].

3. WEAK FORMULATION OF XS-FEM AND DISCRETIZATION

3.1. Strong form and weak form

A two-dimensional solid problem with small displacements in the domain Ω bounded by $\partial\Omega$ is considered. At each point $\mathbf{x}\in\Omega$, the differential forms of the governing equations yield (14) with stresses $\boldsymbol{\sigma}$ and body forces $\mathbf{b}$ and boundary conditions given in (15) and (16):

$$\nabla\cdot\boldsymbol{\sigma} + \mathbf{b} = 0 \quad \text{in } \Omega \tag{14}$$

$$\mathbf{u} = \bar{\mathbf{u}} \quad \text{on } \partial\Omega_u \tag{15}$$

$$\boldsymbol{\sigma}\cdot\mathbf{n} = \bar{\mathbf{t}} \quad \text{on } \partial\Omega_t \tag{16}$$

In the above, the superposed bar denotes prescribed boundary values, $\mathbf{n}$ is the unit normal to the boundary $\partial\Omega_t$ and $\bar{\mathbf{t}}$ is the prescribed traction. On the crack, we assume traction-free surfaces so

$$\boldsymbol{\sigma}\cdot\mathbf{n} = 0 \quad \text{on } \Gamma_C \tag{17}$$

Under the assumption of small strain and displacement, the kinematic equations consist of the strain–displacement relations

$$\boldsymbol{\varepsilon} = \boldsymbol{\varepsilon}(\mathbf{u}) = \nabla_{\mathrm{s}}\mathbf{u} \tag{18}$$

where ∇_{s} is the symmetric part of the gradient operator. If a linear elastic constitutive law is considered then the constitutive relation is

$$\boldsymbol{\sigma} = \mathbf{C} : \boldsymbol{\varepsilon} \tag{19}$$

where $\mathbf{C}$ is the Hookean tensor.

The discrete equations are constructed by the Galerkin method. Consider an admissible function space for the governing equations (14)–(16). A kinematically admissible function space can be defined as follows:

$$U = \{\mathbf{u}\in V(\Omega) \mid \mathbf{u} = \bar{\mathbf{u}} \text{ on } \partial\Omega_u, \quad \mathbf{u} \text{ discontinuous on } \Gamma_{\mathrm{C}}\} \tag{20}$$

The space $V(\Omega)$ allows for discontinuous function across the Γ_C. The test function space is similarly taken as

$$\delta U = \{\delta \mathbf{u} \in V(\Omega) \mid \delta \mathbf{u} = 0 \text{ on } \partial\Omega_u, \quad \delta \mathbf{u} \text{ discontinuous on } \Gamma_C\} \tag{21}$$

where the functions $\delta \mathbf{u} \in \delta U$ vanish on $\partial\Omega_u$.

The potential energy for the given strong form (14)–(16) is

$$\begin{aligned}\Pi(\mathbf{u}) &= \frac{1}{2} a(\mathbf{u}, \mathbf{u})_\Omega - G(\mathbf{u})_\Omega - (\bar{\mathbf{t}}, \mathbf{u})_{\partial\Omega_t} \\ &= \frac{1}{2} \int_\Omega \boldsymbol{\varepsilon}(\mathbf{u}) : \boldsymbol{\sigma}(\mathbf{u}) \, \mathrm{d}\Omega - \int_\Omega \mathbf{u} \bullet \mathbf{b} \, \mathrm{d}\Omega - \int_{\partial\Omega_t} \mathbf{u} \bullet \bar{\mathbf{t}} \, \mathrm{d}\Gamma, \quad \forall \mathbf{u} \in \delta U\end{aligned} \tag{22}$$

in which displacement field $\mathbf{u}$ that minimizes the above functional should be found; it equivalently satisfies the given partial differential equations. Now, setting the first variation of the above functional to zero, i.e. $\delta\Pi(\mathbf{u}, \delta\mathbf{u}) = 0$, a weak form of the given governing equation is obtained by

$$\begin{aligned}\delta\Pi(\mathbf{u}, \delta\mathbf{u}) &= a(\mathbf{u}, \delta\mathbf{u})_\Omega - G(\delta\mathbf{u})_\Omega - (\bar{\mathbf{t}}, \delta\mathbf{u})_{\partial\Omega_t} \\ &= \int_\Omega \boldsymbol{\varepsilon}(\delta\mathbf{u}) : \boldsymbol{\sigma}(\mathbf{u}) \, \mathrm{d}\Omega - \int_\Omega \delta\mathbf{u} \bullet \mathbf{b} \, \mathrm{d}\Omega - \int_{\partial\Omega_t} \delta\mathbf{u} \bullet \bar{\mathbf{t}} \, \mathrm{d}\Gamma, \quad \forall \delta\mathbf{u} \in \delta U\end{aligned} \tag{23}$$

From the predefined test function space (21), the solution $\mathbf{u}$ is obtained by solving the above weak form.

3.2. Discrete system

Consider finite-dimensional subspaces spanned by the basis taken from the test function space. The finite-dimensional subspaces should be chosen to be linearly independent by avoiding coincident elements in the basic and overlaid meshes. When the overlaid mesh is superimposed on the basic mesh, the elements of the basic and overlaid meshes should not coincide. For a given enrichment function $\Psi(\mathbf{x})$, the finite-dimensional subspace $\hat{W}$ is defined by

$$\hat{W} = \mathrm{span}\left\{ \bigcup_{I \in \Lambda} N_I(\mathbf{x}) \oplus \bigcup_{J \in \Lambda_{\mathrm{disc}}} N_J(\mathbf{x})\Psi(\mathbf{x}) \right\}, \quad \mathbf{x} \in \Omega \tag{24}$$

and the finite-dimensional subspace $\hat{W}^{\mathrm{ov}}$ is defined by

$$\hat{W}^{\mathrm{ov}} = \mathrm{span}\left\{ \bigcup_{K \in \Lambda^{\mathrm{ov}}} N_K^{\mathrm{ov}}(\mathbf{x}) \right\}, \quad \mathbf{x} \in \Omega^{\mathrm{ov}} \tag{25}$$

Then, the finite-dimensional subspaces $\hat{W}$ and $\hat{W}^{\mathrm{ov}}$ have the following property:

$$\hat{W}(\Omega) \cap \hat{W}^{\mathrm{ov}}(\Omega^{\mathrm{ov}}) = 0 \tag{26}$$

In this scenario, the interpolation space of the overlapped domain can be enriched by the direct sum of two finite-dimensional subspaces as follows:

$$\hat{W}^{\mathrm{en}}(\Omega^{\mathrm{en}}) = \hat{W}^{\mathrm{ba}} \oplus \hat{W}^{\mathrm{ov}} \tag{27}$$

where Ω^{en} denotes the overlapped domain, i.e. $\Omega^{\mathrm{en}} = \Omega \cap \Omega^{\mathrm{ov}}$ when Ω includes all overlaid domains such that $\Omega^{\mathrm{ov}} \subset \Omega$.

The discrete system of equations are constructed from the standard weak form (23). The test function can be written in discrete form

$$\delta\hat{\mathbf{u}}(\mathbf{x}) = \sum_{I\in\Lambda} N_I(\mathbf{x})\delta\mathbf{u}_I + \sum_{J\in\Lambda_{\mathrm{disc}}} N_J(\mathbf{x})\Psi(\mathbf{x})\delta\mathbf{a}_J + \sum_{K\in\Lambda^{\mathrm{ov}}} N_K^{\mathrm{ov}}(\mathbf{x})\delta\mathbf{c}_K \tag{28}$$

Substituting above test function into (23), the arbitrariness of $\delta\mathbf{u}_I$, $\delta\mathbf{a}_J$ and $\delta\mathbf{c}_K$ yields

$$\int_\Omega \mathbf{B}(\mathbf{x}) : \boldsymbol{\sigma}(\hat{\mathbf{u}})\,\mathrm{d}\Omega = \int_\Omega \mathbf{N}(\mathbf{x}) \bullet \mathbf{b}\,\mathrm{d}\Omega + \int_{\partial\Omega_t} \mathbf{N}(\mathbf{x}) \bullet \bar{\mathbf{t}}\,\mathrm{d}\Gamma \tag{29}$$

$$\int_{\Omega^{\mathrm{ov}}} \mathbf{B}^{\mathrm{ov}}(\mathbf{x}) : \boldsymbol{\sigma}(\hat{\mathbf{u}})\,\mathrm{d}\Omega = \int_{\Omega^{\mathrm{ov}}} \mathbf{N}^{\mathrm{ov}}(\mathbf{x}) \bullet \mathbf{b}\,\mathrm{d}\Omega + \int_{\partial\Omega_t^{\mathrm{ov}}} \mathbf{N}^{\mathrm{ov}}(\mathbf{x}) \bullet \bar{\mathbf{t}}\,\mathrm{d}\Gamma \tag{30}$$

where

$$\mathbf{B}(\mathbf{x}) = \sum_{I\in\Lambda} \frac{\partial N_I(\mathbf{x})}{\partial\mathbf{x}} + \sum_{J\in\Lambda_{\mathrm{disc}}} \frac{\partial(N_J(\mathbf{x})\Psi(\mathbf{x}))}{\partial\mathbf{x}} \tag{31}$$

$$\mathbf{N}(\mathbf{x}) = \sum_{I\in\Lambda} N_I(\mathbf{x}) + \sum_{J\in\Lambda_{\mathrm{disc}}} N_J(\mathbf{x})\Psi(\mathbf{x}) \tag{32}$$

$$\mathbf{B}^{\mathrm{ov}}(\mathbf{x}) = \sum_{K\in\Lambda^{\mathrm{ov}}} \frac{\partial N_K^{\mathrm{ov}}(\mathbf{x})}{\partial\mathbf{x}} \tag{33}$$

$$\mathbf{N}^{\mathrm{ov}}(\mathbf{x}) = \sum_{K\in\Lambda^{\mathrm{ov}}} N_K^{\mathrm{ov}}(\mathbf{x}) \tag{34}$$

As seen in (29) and (30), the equilibrium equations are coupled through the dependence of the stress on both fields. The discrete system of equations can be written as

$$\begin{bmatrix} \mathbf{K}^{\mathrm{ba-ba}} & \mathbf{K}^{\mathrm{ba-ov}} \\ \mathbf{K}^{\mathrm{ov-ba}} & \mathbf{K}^{\mathrm{ov-ov}} \end{bmatrix} \begin{Bmatrix} \mathbf{u}^{\mathrm{ba}} \\ \mathbf{u}^{\mathrm{ov}} \end{Bmatrix} = \begin{Bmatrix} \mathbf{f}_{\mathrm{ext}}^{\mathrm{ba}} \\ \mathbf{f}_{\mathrm{ext}}^{\mathrm{ov}} \end{Bmatrix} \tag{35}$$

where the unknown coefficient vectors are written in the form $\{\mathbf{u}^{\mathrm{ba}}\}^{\mathrm{T}} = \{(\mathbf{u}_1, \ldots, \mathbf{u}_I, \ldots), (\mathbf{a}_1, \ldots \mathbf{a}_J, \ldots)\}^{\mathrm{T}}$ for the basic mesh and $\{\mathbf{u}^{\mathrm{ov}}\}^{\mathrm{T}} = \{(\mathbf{c}_1, \ldots, \mathbf{c}_K, \ldots)\}^{\mathrm{T}}$ for the overlaid mesh. The force vectors $\mathbf{f}_{\mathrm{ext}}^{\mathrm{ba}}$ and $\mathbf{f}_{\mathrm{ext}}^{\mathrm{ov}}$ are calculated from the right-hand sides of (29) and (30), respectively. The components of the stiffness matrix in (35) are given by

$$\mathbf{K}_{IJLM}^{\mathrm{ba-ba}} = \int_\Omega (\mathbf{B}_{IJ}(\mathbf{x}))^{\mathrm{T}} \mathbf{C} \mathbf{B}_{LM}(\mathbf{x})\,\mathrm{d}\Omega \tag{36}$$

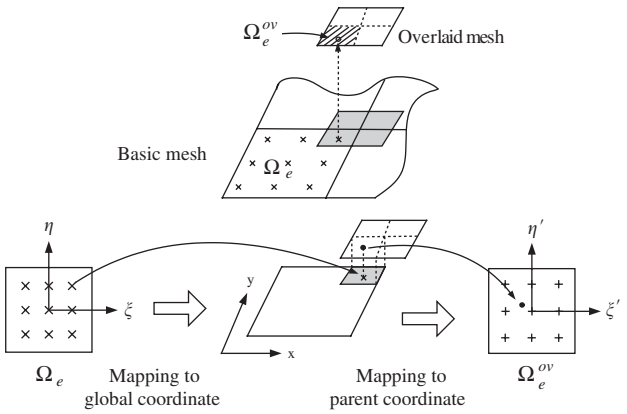

Figure 3. Mapping procedure from the parent co-ordinate (ξ, η) of basic mesh to the other parent co-ordinate (ξ', η') of overlaid mesh for the quadrature of weak form and the measurement of displacement and stress fields.

$$\mathbf{K}_{IJN}^{\text{ba–ov}} = \int_{\Omega} (\mathbf{B}_{IJ}(\mathbf{x}))^{\mathrm{T}} \mathbf{C} \mathbf{B}_{N}^{\text{ov}}(\mathbf{x})\, \mathrm{d}\Omega \tag{37}$$

$$\mathbf{K}_{KLM}^{\text{ov–ba}} = \int_{\Omega^{\text{ov}}} (\mathbf{B}_{K}^{\text{ov}}(\mathbf{x}))^{\mathrm{T}} \mathbf{C} \mathbf{B}_{LM}(\mathbf{x})\, \mathrm{d}\Omega \tag{38}$$

$$\mathbf{K}_{KN}^{\text{ov–ov}} = \int_{\Omega^{\text{ov}}} (\mathbf{B}_{K}^{\text{ov}}(\mathbf{x}))^{\mathrm{T}} \mathbf{C} \mathbf{B}_{N}^{\text{ov}}(\mathbf{x})\, \mathrm{d}\Omega \tag{39}$$

We note that in the XS-FEM, the discrete system of equations retains the symmetry as well as sparsity.

3.3. Numerical integration of the weak form

In integrating the weak form over the overlapped elements, difficulties might arise in numerical quadrature because the integrand is not continuous in those elements. One of the difficulties comes from the fact that the Gauss quadrature points of basic and overlaid meshes do not coincide due to the arbitrary patching of the overlaid mesh corresponding to crack tip. At first glance, the subdivision of the intersected basic elements along the edges of the overlaid elements might be a good approach, but the subdivision of these elements is practically quite awkward. In this work, we used a high order of the Gauss quadrature for the overlaid mesh for the discontinuous integrands of (37) or (38).

In addition, as shown in Figure 3, when the integrands are evaluated over the overlapped elements, the parent co-ordinate of one mesh needs to be mapped to that of the other mesh. For example, the coupled stress in (30) is computed through a double mapping where the parent co-ordinate of basic mesh is first mapped to the global co-ordinate and the global co-ordinate is then mapped to the parent co-ordinate of overlaid mesh again. This double mapping technique is also needed in computing of displacement and stress fields. Fish [9] used a similar mapping

technique in his s-version of finite element method and showed that the mapping is sufficiently accurate in the quadrature of weak form.

The other difficulty arises from the quadrature of the weak form for the elements cut by crack. The contribution of the discontinuous approximation enriched by the step function $\Psi(\mathbf{x})$ should be accurately reflected on the quadrature. In XFEM [2–5, 15], element quadrature has been implemented by creating subdomains on the both sides of the discontinuity; Iarve [16] has proposed a regularization for the integrands. In this work, the elements cut by crack are partitioned into subtriangles whose boundaries align with the crack geometry and the elements consist of the sum of the subtrianlges Ω_d^{sub} as follows:

$$\Omega^{\text{cut}} = \bigcup_{d \in E_e^{\text{cut}}} \Omega_d^{\text{sub}} \tag{40}$$

where E_e^{cut} denotes the total ordering of the subtriangles in the elements on the basic mesh. We note that the subtriangles are required not for additional degree of freedoms related to their subdivisions but for more accurate numerical integration.

3.4. Modelling of crack opening and propagation

In the proposed method, the crack is modelled by the combination of the XFEM and SFEM. Figure 4(a) shows that actual crack opening is measured by the sum of the crack openings of XFEM and SFEM. However, as shown in Figure 4(b), the crack closes ahead of the actual crack tip in the basic mesh and the approximation enriched by the step function does not reach the actual tip. Thus, it is necessary to include a transition region where the approximations of the crack opening by XFEM and SFEM are both operative. Figure 4(c) illustrates the crack opening on the overlaid mesh. Although the crack opening is closed at the element edge to satisfy (3), the sum of two openings constitutes the actual crack opening.

The proposed method provides a useful scheme for the modelling of growing crack. As shown in Figure 5, the tracking of changing crack geometry requires only translation or rotation of the overlaid mesh and the update of the nodes to be enriched by step functions, The s-method [9, 10], on the other hand involves mesh operations such as element insertions or partial remeshing. In the XS-FEM, no intermediate elements need to be inserted in modelling crack growth.

4. NUMERICAL EXAMPLES

4.1. Square patch with near-tip field

To demonstrate the performance of the proposed method, several solutions are described. The first is a square patch with boundary conditions from the closed-form solution for mode I crack problem. Along the boundaries of the patch the known near-tip field tractions (41) and (42) are prescribed and resultant displacement and stress fields are compared with the closed-form solutions [17].

$$\sigma_{xx} = \frac{K_I}{\sqrt{2\pi r}} \cos\left(\frac{\theta}{2}\right)\left[1 - \sin\left(\frac{\theta}{2}\right)\sin\left(\frac{3\theta}{2}\right)\right] \tag{41}$$

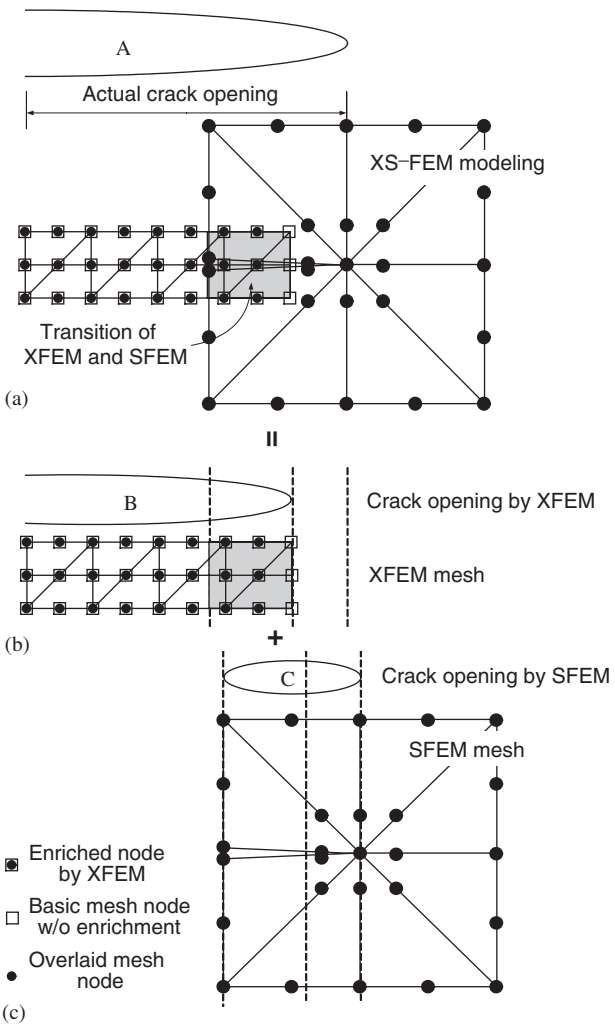

Figure 4. Modelling of a crack opening displacement ($A = B+C$): (a) actual crack opening and its modelling by XS-FEM; (b) crack opening by discontinuous enrichment of the XFEM on the basic mesh; and (c) crack opening by the SFEM on the overlaid mesh.

$$\sigma_{yy} = \frac{K_I}{\sqrt{2\pi r}} \cos\left(\frac{\theta}{2}\right)\left[1 + \sin\left(\frac{\theta}{2}\right)\sin\left(\frac{3\theta}{2}\right)\right] \tag{42}$$

As illustrated in Figure 6 the basic mesh consists of 1018 quadratic triangular elements for 2105 nodes and the overlaid mesh consists of eight coalesced quarter point elements. The stress intensity factor is prescribed as $K_I = 1.0\,\text{psi}\sqrt{\text{in}}$ and is recalculated by the interaction integral [18]. Figures 7(a) and 7(b) show that the crack opening displacement and near-tip stress agree well with the closed-form solutions. A stress contour plot of Figure 8 shows that the stress

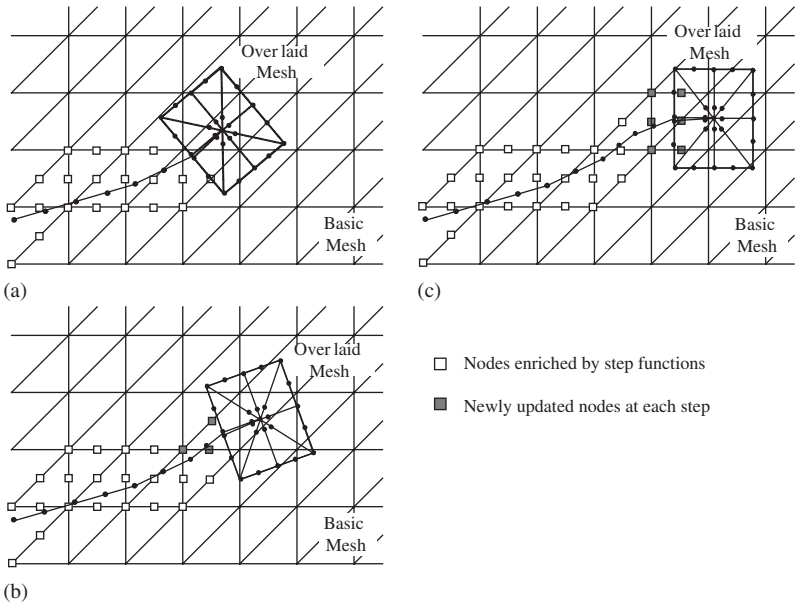

Figure 5. Modelling of crack propagation in the XS-FEM; an overlaid mesh is translated or rotated and enriched nodes are updated in a basic mesh at steps (a)–(c).

field is characterizing a crack is successfully captured. Also, the relative error of the computed stress intensity factor is within 0.39%.

4.2. Edge crack under tension and shear

Figure 9(a) shows an edge-cracked specimen under uniform tension $\sigma_y = 1$ psi for mode I state. Figure 9(b) illustrates a mixed-mode loading where the top of the plate is subjected to uniform shear $\tau = 1.0$ psi and the bottom is fixed. In both problems, plane stress case is assumed; Young's modulus $E = 3 \times 10^7$ psi and Poisson's ratio $v = 0.25$. The same mesh structure shown in Figure 10 is used in both cases, which consists of an unstructured basic mesh of 1149 nodes and 2238 linear triangular elements and an overlaid mesh with a set of quarter point elements.

The stress intensity factor for mode I is compared to the analytic solutions by Tada *et al.* [19] in Table I and shows very good agreement. In Table II, the stress intensity factors for mixed-mode states are compared with the reference solutions that have been given in Reference [20]. The comparison also shows very good accuracy.

4.3. Edge crack with variation of slant angles

This example as shown in Figure 11(a) examines the edge crack under tension with various slant angles; 0, 30, 45 and 60°. Figure 11(b) shows one of the meshes for the 30° slant crack. A total of 2366 nodes are used in the basic mesh. In the other meshes, the overlaid mesh is translated and rotated to align with the crack tip.

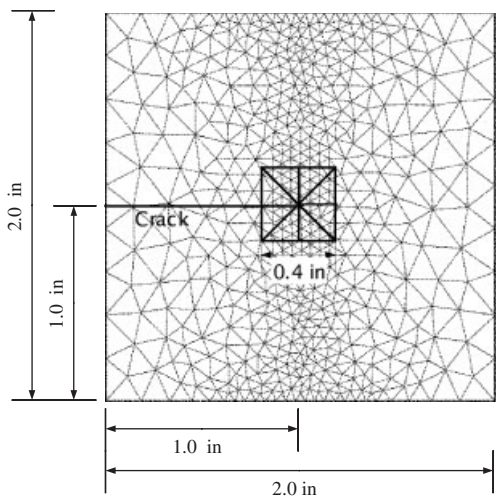

Figure 6. A square patch with near-tip field and the mesh structure.

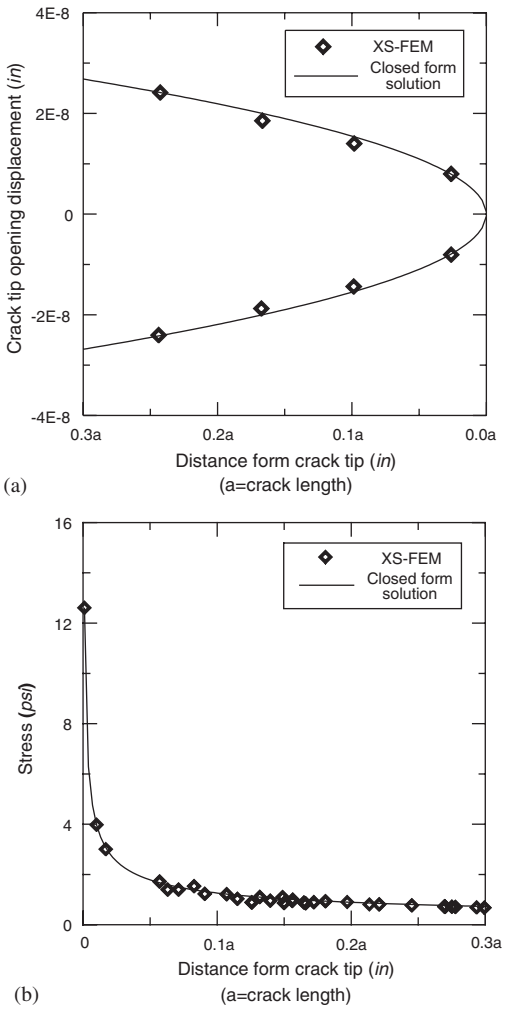

Figure 7. Comparison of displacement and stress profiles of square patch with near-tip field to the closed form solutions: (a) crack tip opening displacement (u_y); and (b) stress (σ_y).

Table III compares the stress intensity factors with the reference solutions presented by Tada *et al.* [19]. The stress intensity factors show excellent agreements with the reference solutions for all of the slant angles. In all cases, the relative errors are less than 1%.

4.4. Slant crack growth simulation

In this section, the effectiveness of modelling crack growth is demonstrated. As shown in Figure 12, 45° slanted edge-cracked specimen under uniform tension ($\sigma_y = 1\,\text{psi}$) is considered.

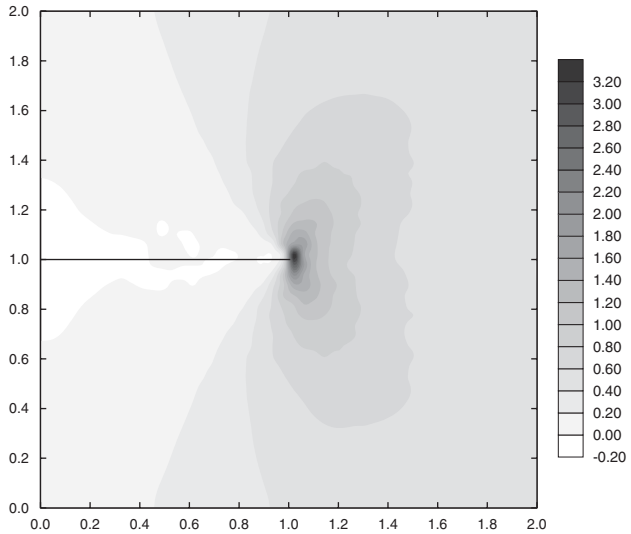

Figure 8. Stress (σ_y) contour plot of square patch with near-tip fields (unit: psi).

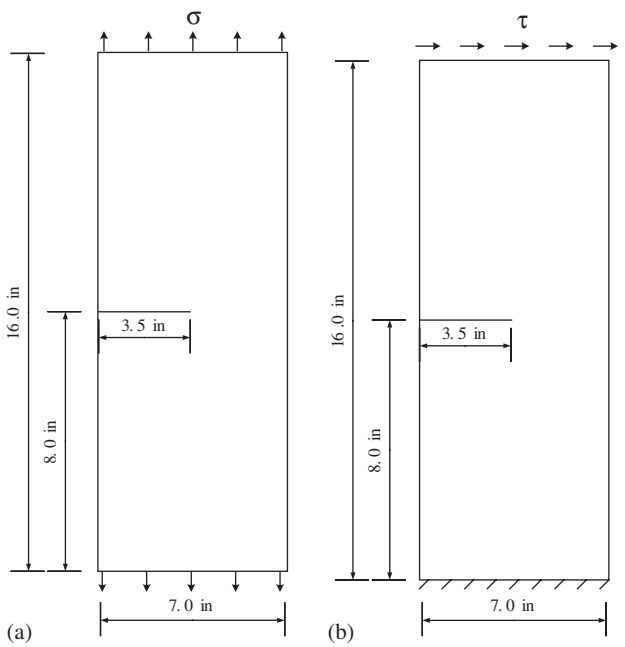

Figure 9. Problem illustrations: (a) edge-cracked specimen under tension; and (b) edge-cracked specimen under shear.

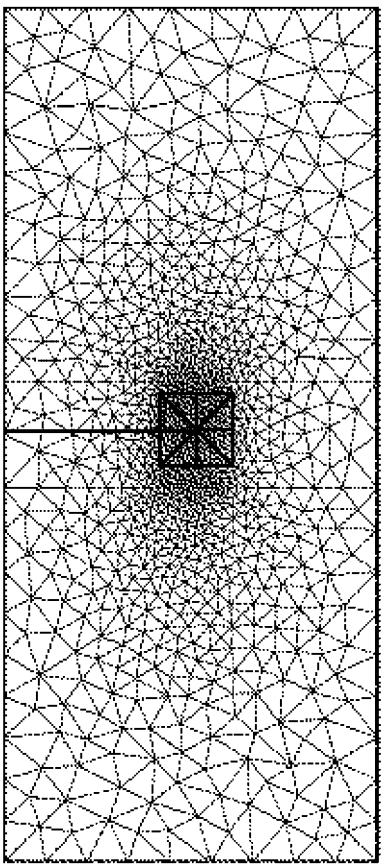

Figure 10. Basic and overlaid meshes for edge-cracked specimen under uniform tension and shear.

Table I. Stress intensity factor of edge crack under tension.

	Reference solution	XS-FEM	Relative error (%)
Mode I SIF	9.37	9.34	0.27

The initial mesh consists of the basic mesh with 1154 nodes, 2218 linear triangular elements and the overlaid mesh. The material has the same properties as previous examples.

The crack increment of each step is determined by the Paris law for fatigue crack growth and the direction of crack extension is computed by the maximum hoop stress criterion [21]. Figure 13 shows the final configuration of the crack path after growing 14 steps. The crack path is successfully predicted without noticeable oscillation by the modelling technique presented in Section 3.4. Figure 14 shows modes I and II stress intensity factors as a function of the length of the crack. Mode I effect becomes dominant as the crack grows whereas the mode II effect diminishes rapidly.

Table II. Stress intensity factors of edge crack under shear.

	Reference solution	XS-FEM	Relative error (%)
Mode I SIF	34.00	34.10	0.29
Mode II SIF	4.55	4.50	1.10

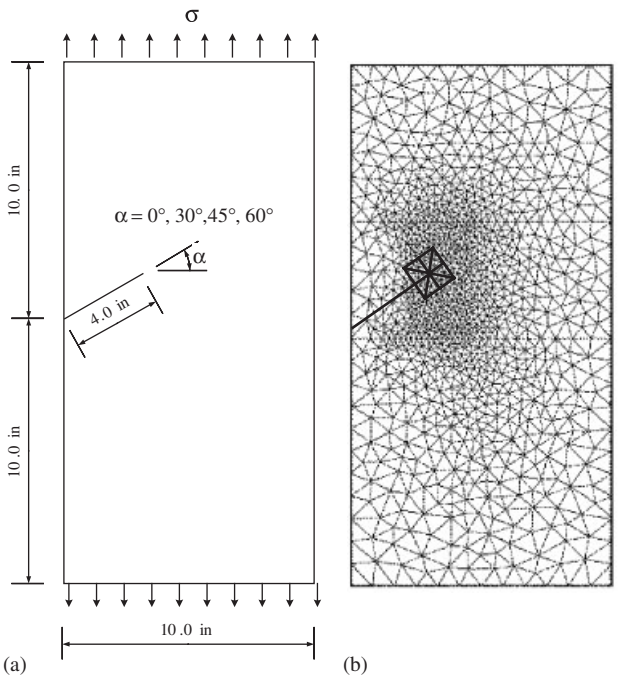

Figure 11. Edge crack with variation of slant angles under tension: (a) problem description; and (b) basic and overlaid meshes.

5. CONCLUSIONS

This paper has developed a hybrid method called XS-FEM for modelling cracks, in which the crack tip is treated by a superimposed patch (overlaid mesh) consisting of quarter point elements and the rest of the crack is treated by the XFEM. The mesh superposition technique (SFEM) is used to match the near-tip fields with discontinuous displacement field of the basic mesh. The proposed method simplifies the difficulty in integration of near-tip fields that matches with the step function. Furthermore, a local partition of unity does not lose the reproducing property when the enriched elements are blended with standard finite elements, and interpolation spaces are well defined when the near-tip field matches with enriched displacement field because the near-tip field totally participates in the complete approximation avoiding linear dependency.

Table III. Stress intensity factors according to the variation of slant crack angles.

Slant angles	Mode	Reference solutions	XS-FEM	Relative errors (%)
0°	Mode I	7.75	7.73	0.26
	Mode II	—	—	—
30°	Mode I	5.54	5.55	0.18
	Mode II	1.72	1.71	0.58
45°	Mode I	3.66	3.64	0.55
	Mode II	1.79	1.78	0.56
60°	Mode I	2.10	2.08	0.95
	Mode II	1.48	1.49	0.68

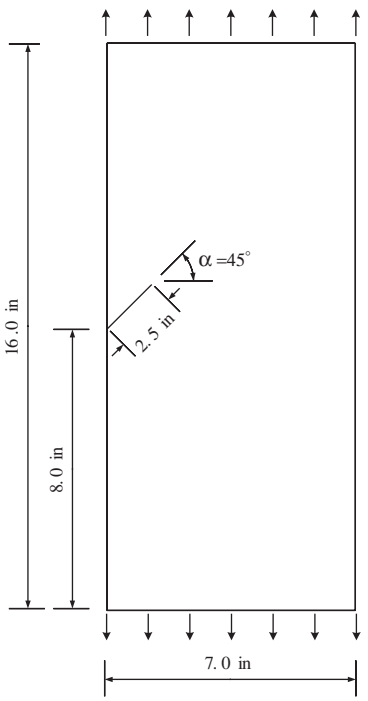

Figure 12. Problem description for modelling growth of slanted edge crack in a plate under tension.

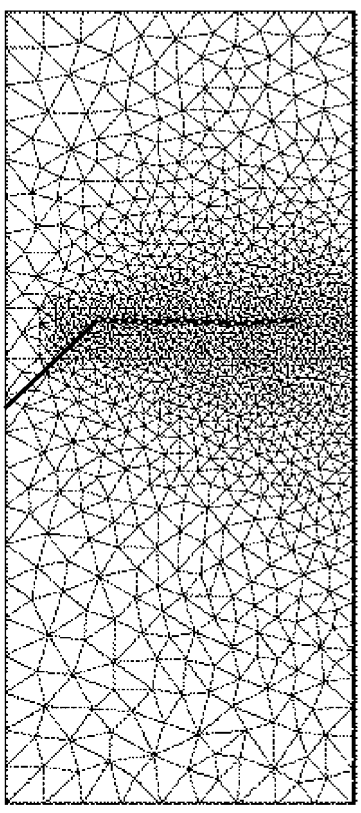

Figure 13. Final configuration of slanted edge crack after growing under tension.

The quadrature of the weak form where the integrand is discontinuous due to arbitrary overlap of mesh was effectively dealt with by double mapping procedure. The description of actual crack opening can be achieved by coupled approximations of XFEM and SFEM.

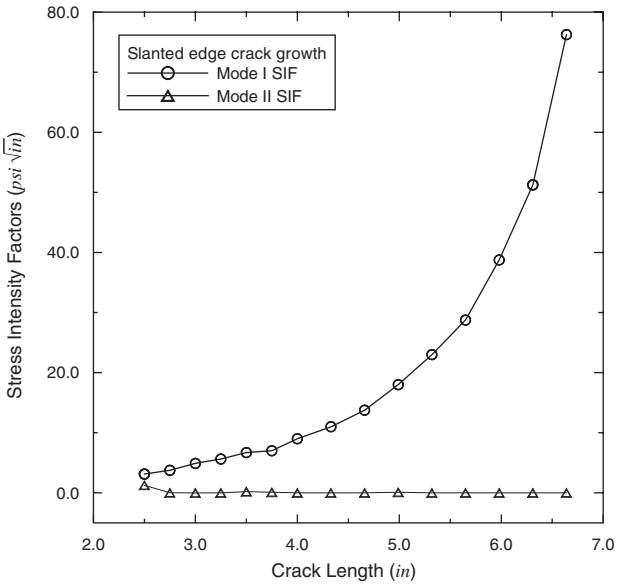

Figure 14. Modes I and II stress intensity factors as a function of the length of the crack.

The crack growth is modelled by the translation and rotation of the overlaid mesh and the update of enriched nodes on the basic mesh. This feature makes the method attractive for crack growth computations where otherwise burdensome remeshing would be needed. The proposed method easily treats the changing geometry due to crack growth and can be generalized to other problems such as those relating to beams, plates, shells and three-dimensional problems.

ACKNOWLEDGEMENTS

This work was supported by Korea Research Foundation Grant (KRF-2002-042-D00115) and the U.S. Office of Naval Research.

REFERENCES

1. Melenk JM, Babuska I. The partition of unity finite element method: Basic theory and application. *Computer Methods in Applied Mechanics and Engineering* 1996; **139**:289–314.
2. Moës N, Dolbow J, Belytschko T. A finite element method for crack growth without remeshing. *International Journal for Numerical Methods in Engineering* 1999; **46**:131–150.
3. Moës N, Dolbow J, Belytschko T. Discontinuous enrichment in finite elements with a partition of unity method. *Finite Elements in Analysis and Design* 2000; **36**:235–260.
4. Daux C, Moës N, Dolbow J, Sukumar N, Belytschko T. Arbitrary branched and intersecting cracks with the eXtended Finite Element Method. *International Journal for Numerical Methods in Engineering* 2000; **48**: 1741–1760.
5. Belytschko T, Moës N, Usui S, Sukumar N, Parimi C. Arbitrary discontinuities in finite element. *International Journal for Numerical Methods in Engineering* 2001; **50**:993–1013.
6. Moës N, Belytschko T. Extended finite element method for cohesive crack growth. *Engineering Fracture Mechanics* 2002; **69**:813–833.

7. Zi G, Belytschko T. New crack-tip elements for XFEM and applications to cohesive cracks. *International Journal for Numerical Methods in Engineering* 2003; **57**:2221–2240.
8. Stazi F, Budyn E, Chessa J, Belytschko T. XFEM for fracture mechanics with quadratic elements. *Computational Mechanics* 2003; **31**:38–48.
9. Fish J. The s-version of the finite element method. *Computers and Structures* 1992; **43**:539–547.
10. Fish J, Nath A. Adaptive and hierarchical modelling of fatigue crack propagation. *International Journal for Numerical Methods in Engineering* 1993; **36**:2825–2836.
11. Fish J, Guttal R. The s-version of finite element method for laminated composites. *International Journal for Numerical Methods in Engineering* 1996; **39**:3641–3662.
12. Belytschko T, Fish J, Bayliss A. The spectral overlay on finite elements for problems with high gradients. *Computer Methods in Applied Mechanics and Engineering* 1990; **81**:71–89.
13. Chessa J, Wang H, Belytschko T. On the construction of blending elements for local partition of unity enriched finite elements. *International Journal for Numerical Methods in Engineering* 2003; **57**:1015–1038.
14. Barsoum RS. On the use of isoparametric finite elements in linear fracture mechanics. *International Journal for Numerical Methods in Engineering* 1976; **10**:25–37.
15. Sukumar N, Chopp DL, Moës N, Belytschko T. Modeling holes and inclusions by level sets in the extended finite-element method. *Computer Methods in Applied Mechanics and Engineering* 2001; **190**:6183–6200.
16. Iarve EV. Mesh independent modelling of cracks by using higher order shape functions. *International Journal for Numerical Methods in Engineering* 2003; **56**:869–882.
17. Fleming M, Chu YA, Moran B, Belytschko T. Enrichment element-free Galerkin methods for crack tip fields. *International Journal for Numerical Methods in Engineering* 1997; **40**:1483–1504.
18. Moran B, Shih CF. Crack tip and associated domain integrals from momentum and energy balance. *Engineering Fracture Mechanics* 1987; **27**:615–641.
19. Tada H, Paris PC, Irwin GR. *The Stress Analysis of Cracks Handbook*. Del Research Corporation, Hellertown, PA, 1985.
20. Yau J, Wang S, Corten H. A mixed-mode crack analysis of isotropic solids using conservation laws of elasticity. *Journal of Applied Mechanics* 1980; **47**:335–341.
21. Erdogen F, Shi GC. On the crack extension in plates under loading and transverse shear. *Journal of Basic Engineering* 1963; **85**:519–527.

